2005 유체기계 연구개발 발표회 논문집, pp. 17~40
창원대학교 국제교류센터 및 정보전산원 2005. 12. 1~2

Pressure Fluctuation Prediction by Using Turbulent Flow Analysis in Francis Turbine

By Wu Yulin , Dept. of Thermal Engineering, Tsinghua University, Beijing, China

Flow in a hydraulic turbine is known to be unsteady due to flow instabilities and mutual interactions between the rotating part and the stationary parts. Flow instabilities are mostly viscous phenomena such as boundary layer separation and vortex shedding that produces relatively low frequency and small amplitude pressure fluctuations. This kind of flow unsteadiness is important because it affects the efficiency and causes fluctuation on power output. Mutual interaction between the runner blades and the guide vanes produces relatively high frequency and large amplitude pressure fluctuations. This phenomenon is more closely related to compressibility than viscosity. It is important because it may cause structural vibration and noise.

In this paper, the unsteady turbulent flow through the whole flow passage of an entire turbine, that is, from the flow inlet of the machine to the outlet as a unique calculation domain, has been computed to predict the pressure fluctuation of flow in the hydraulic machinery.

1 Introduction to Pressure Fluctuation Prediction by Using Unsteady Turbulent Flow Analysis

In hydraulic machinery, many problems arise due to dynamical effects and vibrations. Dynamical forces can not be obtained by the steady state approach. Also the measurement of the dynamical forces is quite complicate and requires a rather high measuring effort. Therefore it is desirable to obtain it by numerical simulation. For the calculation of these dynamical effects it is essential to apply an unsteady flow calculation including the stator-rotor interaction. Due to the nonuniform inflow from the spiral case and due to the unequal pitching of guide vanes and runner it is necessary to consider the entire turbine with all channels of the runner and of the tandem cascade. In this paper the unsteady turbulent flow simulation of the entire water turbine is shown. The investigated turbine consists of spiral case, stay vanes guide vanes, runner with several blades and draft tube.

1.1 Unsteadiness of Flow through Turbines

For more than a decade Computational Fluid Dynamics (CFD) has been used in hydraulic machinery for research and development. Early successful demonstrations were given, for example, in the GAMM workshop [1]. Today usually the Reynolds averaged Navier-Stokes equations together with a robust model of turbulence model (usually the $k\varepsilon$ model) is used. It is common practice to apply steady flow simulations. However, the actual flows in hydraulic machinery are unsteady phenomena [2, 3]. Two major groups of unsteady problems can be distinguished. The first group is flows with an externally forced unsteadiness. This can be caused by unsteady boundary conditions or by changing of the geometry with time, for example, the rotor-stator interactions in hydraulic machines. The second group is flows with self excited unsteadiness, which are e. g. turbulent motion, vortex shedding (Karman vortex street) or unsteady vortex behavior (e. g. vortex rope in a draft tube). Here the unsteadiness is obtained without any change of the boundary conditions or of the geometry. There can also occur a combination of both groups (e. g. flow induced vibrations, change of geometry caused by vortex shedding) [4, 5]. The following is the examples of unsteady flows in hydraulic machinery [6].

1.1.1 Vortex rope in a draft tube

As an self excited unsteady flow example, the simulation of a vortex rope in a draft tube is shown. Fig. 1-1 shows the photo of vortex rope in draft tube of a hydraulic Francis turbine at a low flow rate working condition. The instantaneous flow for a certain time step of an unsteady flow computation is given in Fig. 1-2, where pressure contours are shown Clearly the cork-screw type flow with an unsymmetrical form is visible, although the geometry and the boundary conditions are completely axisymmetrical.

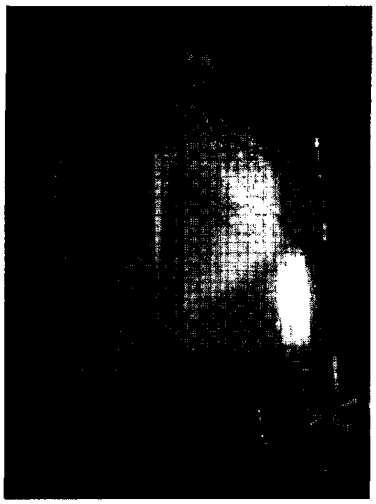

Fig. 1-1 Photo of vortex rope in draft tube of Francis turbine at a low flow rate working condition

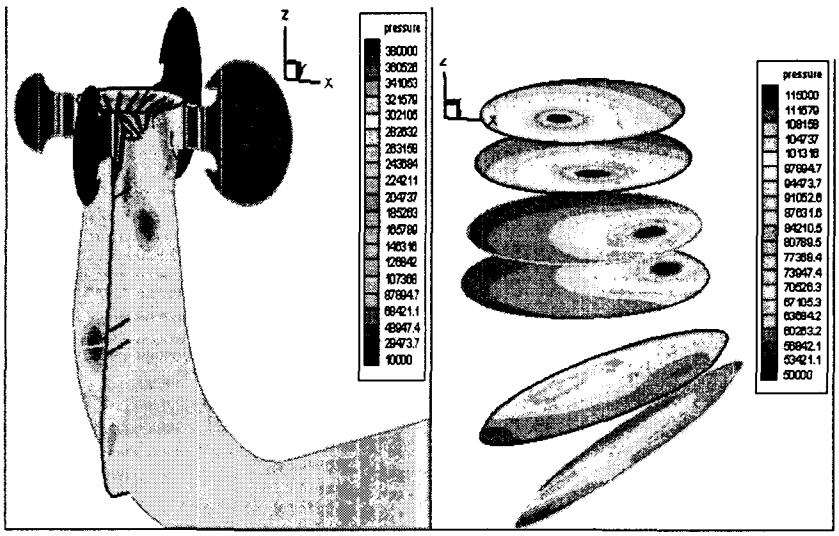

Fig. 1-2 Iso-pressure of a vortex rope in draft tube at low flow rate condition

1.1.2 Vortex instability in a pipe trifurcation

Another unsteady problem caused by a vortex instability is a pipe trifurcation, which is established in power plants. The trifurcation distributes the water from the penstock to several turbine units. The

problem in plant arises from severe fluctuations of the power output of the both outer turbines. But this phenomenon is nou studied in the paper.

1.1.3 Rotor-stator interaction in hydraulic turbine

The following example belongs to the second group, the unsteadiness is forced by moving geometries. Modern designs of hydraulic machinery are driven toward highly compact on figurations. The trend to increase the blade loading and decrease the machine size and weight makes it important to understand the interaction between the guide vanes and the runner. During the optimization process of a runner, with respect to the efficiency, cavitation behavior and pressure pulsation, the interaction between the guide vanes and runner blades is one important point. Fast responses and high accuracy of the used numerical tools are required. Several numerical approaches are useful and provided. There are several possibilities to model the interaction of stationary and rotating part in the flow path of a hydraulic machine.

(1) Simple 'top-down' computation,

(2) Mixing plane approach,

(3) Frozen rotor computation,

(4) Transient computation.

The simplest way to compute the flow in a hydraulic machine is to solve each component in its own frame of reference, taking the results of the upstream component as inlet boundary condition. But there is no interaction between the components and results heavily depend on proper inlet boundary conditions.

One way to account for the interaction is the mixing plane model. In flow field simulations with a so-called stage interface, the flow quantities are circumferentially averaged in a mixing plane between the guide vanes and the runner. Such methods have reached a high degree of maturity. It is assumed that the physical mixing supplied by the relative motion between the components is sufficiently large to cause any upstream velocity profile to mix out prior to entering the downstream components. This can only be true if the physical distance between the components is large enough.

Another steady-state calculation is the frozen rotor calculation. The position of the runner is fixed relative to guide vanes during the calculation. Several different positions of the runner relative to guide vanes must be computed to obtain useful results. This method is able to capture some flow characteristics associated with the guide vanes.

The third way is the full 3D in stationary calculation, which is by far the most physical approach to obtain solutions of the transient flow field in a hydraulic machine. But the fully 3D calculation still requires a lot of CPU time. One of the major problems is the unequal pitch in most hydraulic machines. This leads to the simulation of the whole machine, which is extremely expensive. The detailed computational results will be shown in the following sections.

1.2 Development of Unsteady Flow Simulation through Hydraulic Machinery

For design and research in hydro turbines the application of computational methods is steadily increasing. Nowadays it is fairly standard to simulate the different components separately. By assuming steady state uniform flow conditions in circumferencial direction only one channel of the tandem cascade (stay vanes and guide vanes) and of the runner has to be considered.

Since very often there are strong interactions between the components (especially between guide vanes, runner and draft tube) it is inevitable to introduce this interaction into the simulation for accurate results. Many attempts have been made lately to do this by applying an averaging procedure in the circumferential direction, as described in 1.1.3. This still allows to consider only one channel of tandem cascade and runner and to apply a steady state computation, which results in a severe saving of computer resources. The obtained results agree quite well with measurements and can be applied for turbine design, e.g. [7].

However, many problems arise due to dynamical effects and vibrations. Dynamical forces can not be obtained by the steady state approach. For the calculation of these dynamical effects it is essential to apply an unsteady calculation of flow including the dynamical stator-rotor interaction. Due to the no uniform inflow from the spiral case and due to the unequal pitching of guide vanes and runner it is necessary to consider the entire turbine with all channels of the runner and of the tandem cascade.

Flow in hydraulic machinery is unsteady due to the viscous phenomena such as boundary layer separation and vortex shedding and the mutual interaction between the runner blades and the guide vanes. It is now established that the compressibility effect is important to rapidly changing flows no matter how small the Mach number may be [8]. This is much like the fact that viscosity is important to space wise highly variable flows even when Reynolds number is large. Therefore, for the highly unsteady and turbulent flows, both compressibility and viscosity should be properly taken into account. The developed computational method [9, 10] incorporating the concept of Large Eddy Simulation and based on the Navier-Stokes equations for weakly compressible flows is used to simulate a pump-turbine operating at various conditions including both turbine and pump modes. The computed pressure fluctuation at various locations near guide vanes as well as the runner efficiency is compared with experimental data. Flow instabilities when operated in off design conditions are examined using a numerical flow visualization technique.

2 Basic Equations of Unsteady Flow through Hydraulic Machinery and Turbulence Model

2.1 Basic Equations of Unsteady Flow through Hydraulic Machinery

In fluid mechanics, the basic equations to describe the water flow are the mass continuity equation, the momentum equations (Navier-Stikes equations) and the energy equation. In hydraulic machinery, the coordinate system fixed on runner rotating with the angular

speed ω is chosen, then the relative flow in the runner is steady, and the governing equations of continuity and motion may be written as follows.

$$\nabla \cdot \boldsymbol{W} = 0 \tag{1}$$

$$\frac{\mathrm{D}\boldsymbol{W}}{\mathrm{D}t} = \frac{\partial \boldsymbol{W}}{\partial t} + \boldsymbol{W} \cdot \nabla \boldsymbol{W} = -\frac{\nabla p}{\rho} + \boldsymbol{f} + \frac{\mu}{\rho}\nabla^2 \boldsymbol{W} - \left[2\boldsymbol{\omega} \times \boldsymbol{W} + \boldsymbol{\omega} \times (\boldsymbol{\omega} \times \boldsymbol{R})\right] \tag{2}$$

where $\boldsymbol{W}$ is relative velocity ; $p\rho$ are the pressure and density of the fluid respectively ; $\boldsymbol{f}$ is the mass forceμ is the viscosity , and $\boldsymbol{R}$ is the radius vector. And $-2\boldsymbol{\omega} \times \boldsymbol{W}$ describes the Coriolis force, as well as $-\boldsymbol{\omega} \times (\boldsymbol{\omega} \times \boldsymbol{R})$ the centrifugal force.

But in the absolute coordinate system the continuity equation and the momentum equations (Navier-Stikes equations) are shown by using the absolute velocity $\boldsymbol{V}$ as follows

$$\nabla \cdot \boldsymbol{V} = 0 \tag{3}$$

$$\frac{\mathrm{D}\boldsymbol{V}}{\mathrm{D}t} = \frac{\partial \boldsymbol{V}}{\partial t} + \boldsymbol{V} \cdot \nabla \boldsymbol{V} = -\frac{\nabla p}{\rho} + \boldsymbol{f} + \frac{\mu}{\rho}\nabla^2 \boldsymbol{V} \tag{4}$$

2.2 Turbulence Model for Unsteady Flow Simulation

In the present unsteady turbulent flow simulation, the RNG $k-\varepsilon$, that means Renormalization Group $k-\varepsilon$ turbulence model (k is the turbulent kinetic energy and ε is the turbulent energy dissipation rate) is applied to close the Reynolds equations. The advantages of this model are:

(1) The coefficients in the model were deduced theoretically, do not come from experience.

(2) There is an additional term in the ε equation, which presents the influence of mean strain rate to the turbulent energy dispassion rate.

(3) The RNG $k-\varepsilon$ model can be used to simulate flow separation and vortex.

k and ε equations at the RNG $k-\varepsilon$ model are as follows:

$$\rho\frac{Dk}{Dt} = \frac{\partial}{\partial x_j}\left(\alpha_k \mu_{eff}\frac{\partial k}{\partial x_j}\right) + G_k + G_b - \rho\varepsilon - Y_M \tag{5}$$

$$\rho\frac{D\varepsilon}{Dt} = \frac{\partial}{\partial x_j}\left(\alpha_\varepsilon \mu_{eff}\frac{\partial \varepsilon}{\partial x_j}\right) + C_{1\varepsilon}\frac{\varepsilon}{k}(G_k + C_{3\varepsilon}G_b) - C_{1\varepsilon}\rho\frac{\varepsilon^2}{k} - R \tag{6}$$

where the effective viscosity μ_{eff} is the sum of molecular viscosity μ and the turbulent eddy viscosity μ_t, that is,

$$\mu_{eff} = \mu + \mu_t \tag{7}$$

where

$$\mu_t = C_\mu \frac{k^2}{\varepsilon} \tag{8}$$

And the production of turbulence kinetic energy G_k is:

$$G_k = -\rho \overline{v'_i v'_j} \frac{\partial v_j}{\partial x_i} = \mu_t S^2 \qquad S = \sqrt{2 S_{ij} S_{ij}} \tag{9}$$

where S_{ij} is the strain tensor. And G_b is the turbulence energy production from the buoyancy force, and Y_M is the dissipation caused by the compressibility, but they are not considered in the present computation. The additional term in Eq. (8) is

$$R = \frac{C_\mu \rho \eta^3 (1 - \eta/\eta_o)}{1 + \beta \eta^3} \frac{\varepsilon^2}{k} \tag{10}$$

where $\eta = S\frac{k}{\varepsilon}$, $\eta_o = 4.38$, $C_\mu = 0.0845$, $\beta = 0.012$, $C_{1\varepsilon} = 1.42$, $C_{2\varepsilon} = 1.68$, $\alpha_k = 1.0$, $\alpha_\varepsilon = 0.769$.

At the low Reynolds flow region, the eddy viscosity μ_t can be determined by using the following formulae,

$$d\left(\frac{\rho k^2}{\sqrt{\varepsilon \mu}}\right) = 1.72 \frac{\hat{\mu}}{\sqrt{\hat{\mu}^3 - 1 + C_V}} d\hat{\mu} \tag{11}$$

where $\hat{\mu} = \frac{\mu_{eff}}{\mu}$, $C_V \approx 100$.

2.3 Grid Technology and Numerical Method for Unsteady Flow Simulation

2.3.1 Unstructured grid technology

Recently, research of grid technology is focused on the unstructured grid system. Any spatial calculative domain can be divided to tetrahedron system, which is the simplest element in three dimensional simulation. And this system has strong flexibility and adaptability to any complex domain. The tetrahedron grid system has been used in the present computation of the entire flow passage of hydraulic machinery.

2.3.2 Sliding grid system

Because of the consideration of unsymmetrical flow in spiral case the inflow to tandem cascade and consequently the runner can be unsymmetrical as well. Together with the unequal pitching of guide vanes and runner, this leads to the fact, that no flow periodicity exists. Therefore the complete hydraulic turbine including all flow channels in the tandem cascade and in the runner has to be considered. This represents the most general approach for the prediction of rotor/stator interactions, but it requires huge computational grids. Fig. 2-1 shows a model Francis turbine grid system, which consists of four parts: spiral casing, stay vanes and guide vanes, runner and draft tube. Among them, the runner will be rotating at the unsteady flow calculation.

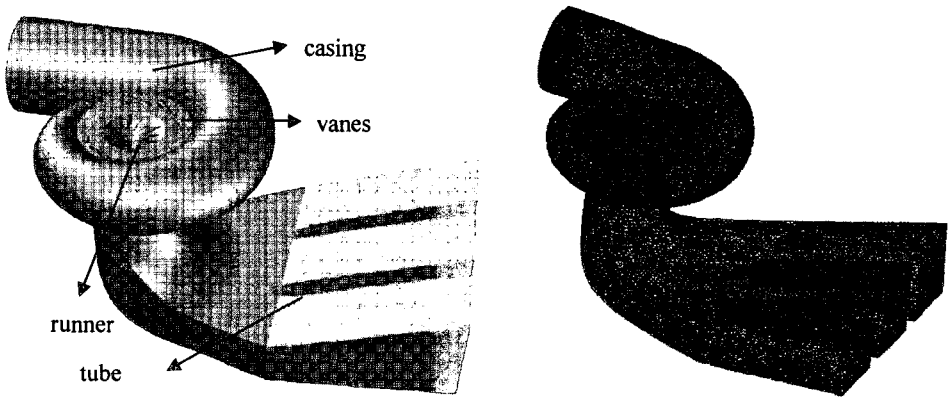

(a) Calculated domain (b) Grid system

Fig.2-1 The model hydraulic turbine

In the unsteady calculation of the entire flow passage of a hydraulic turbine, there are sliding interfaces at the inlet and outlet of a hydraulic turbine runner, as shown in Fig. 2-2. The sliding grid can move along two sides of the interface, on which grid nodes on two side are not necessary to be in superposition to each other. But at the calculation the flux of momentum should be equal at two side of the interface.

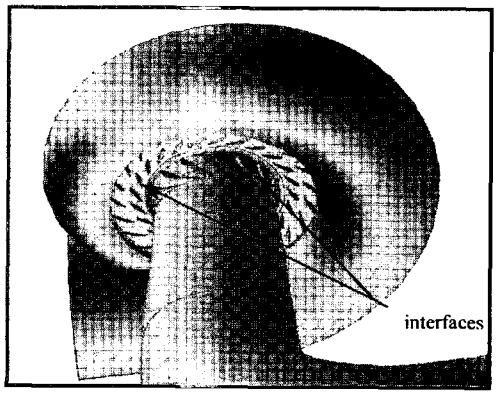

Fig. 2-2 Sliding interfaces at inlet and outlet of runner

2.3.3 Boundary conditions of unsteady calculation in hydraulic turbine

In the calculation of three dimensional turbulent flow through the entire flow passage from the inlet of spiral casing to the outlet of draft tube of a turbine, the following boundary conditions have been used. The similar conditions can be also given for a pump in the entire passage computation.

(1) At the inlet of spiral casing, the pressure value is given. And the same pressure condition is given at the outlet of the draft tube. From the known inlet and outlet pressure, the flow discharge through the turbine will be obtained at final results after many steps of calculated iteration.

(2) At the solid wall, the non-slip flow condition was applied with the wall function near the wall. If the wall is rotating, the circumferential velocity on the wall must be given.

(3) At beginning of calculation, the initial values of velocity, turbulence kinetic energy and energy dissipation rate have been given. In the iterative process the second type of boundary conditions should be given for all physical variables on whole boundaries except the inlet pressure and the outlet pressure, as indicated in (1).

(4) In the iterative process, the correction of the flow discharge will be carried out at the outlet of draft tube of the turbine, which will result in determining of the flow discharge through the turbine in final results.

2.3.4 Numerical approach of unsteady calculation

In this present paper, The time-dependent governing equations must be discretized both in space and time. The unsteady second order implicit formulation is used to calculate the unsteady flow to predict the pressure fluctuation through a turbine and a pump. And the RNG k - ε turbulence model is applied for the unsteady turbulent flow, with the wall function near walls. The finite volume algorithm, with the second order central difference for the source term and with the second order upstream difference for the convective term of the spatial discrete governing equations, is used for numerical simulation. The SIMPLE or the SIMPLEC method are applied for solving the incompressible flow. After getting the variation of pressure with respect to time, the FFT transform is used to get the spectrum of the pressure.

The spatial discretization for the time-dependent equations is identical to the steady-state case by using second order space difference discretization. The temporal discretization involves the integration of every term in the differential equations over a time step Δt. The integration of the transient terms is straightforward, as shown below. A generic expression for the time evolution of a variable ϕ is given by

$$\frac{\partial \phi}{\partial t} = F(\phi)$$

where the function F incorporates any spatial discretization. If the time derivative is discretized using backward differences, the second-order discretization is given by

$$\frac{3\phi^{n+1} - 4\phi^{n} + \phi^{n-1}}{2\Delta t} = F(\phi)$$

where ϕ is a scale quantity; n+1 is the value at the next time level $t + \Delta t$; n is the value at the current time level t; and n-1 is the value at the previous time level $t - \Delta t$.

Once the time derivative has been discretized, a choice remains for evaluating $F(\phi)$. The Implicit Time Integration is to evaluate $F(\phi)$ at the future time level, that is

$$\frac{3\phi^{n+1} - 4\phi^{n} + \phi^{n-1}}{2\Delta t} = F(\phi^{n+1})$$

This is referred to as ``implicit" integration since ϕ^{n+1} in a given cell is related to in neighboring cells through $F(\phi^{n+1})$. Then this implicit equation can be solved iteratively by initializing ϕ^{i} to ϕ^{n} and iterating the equation

$$\phi^{i} = \frac{4}{3}\phi^{n} - \frac{1}{3}\phi^{n-1} + \frac{2}{3}\Delta t F(\phi^{i})$$

for the second-order implicit formulation, until ϕ^{i} stops changing (i.e., converges). At that point, ϕ^{n+1} is set to ϕ^{i}. The advantage of the fully implicit scheme is that it is unconditionally stable with respect to time step size.

2.3.5 The Pressure fluctuation character analysis by using the FFT (Fast Fourier Transform) method

In the unsteady flow computation, the pressure fluctuation amplitude can be recorded at several positions, for example, at the inlet of runner and at the inlet of draft tube at every step of computational time. After finishing the unsteady computation, samples of the pressure fluctuation versus time will be obtained with several hundreds or several thousands data (the number of data is determined by the iterative steps, but at least, it must have 512 data). The sample is the pressure fluctuation amplitude versus time for all frequencies present. Then FFT based spectrum analysis is used, which will provide a display of pressure fluctuation amplitude versus frequency signals, so that the characters of the fluctuation, for example, of the critical frequency can be understand. Of course, one should find the pressure fluctuation sources through the spectrum analysis results.

3 Unsteady Flow Simulation through Hydraulic Turbines

At the off-design operation conditions, flow separation will occur at the inlet of runner blades, which results in the pressure random fluctuation. This fluctuation frequency has not a fixed value. At the small flow rate condition, there is a flow separation near the suction surface of runner blade, this separation is not stable in space and time, causes the pressure fluctuation on blades and induces mechanical vibration of blades.

At the same time, under the off-design operation conditions, the internal flow situation in the runner also is different from the design condition. The exit circulation of flow occurs at the outlet of runner, which results in vortex rope in draft tube. At small discharge condition, the vortex rope rotating with the same direction of the runner will be serious, which induces vibration of draft tube and whole machine. This phenomenon should be predicted by unsteady flow simulation and should be treated to minimize the fluctuation amplitude by changing geometrical parameters of the runner and the draft tube.

The unsteady flow simulation has been carried out in a model Francis turbine, its parameters are listed in Table 1. The steady flow of the turbine has been finished to predict the flow characters, and the energy and cavitation performances. Based on the steady simulation, the unsteady simulation can continue through the entire passage of the turbine from the inlet of spiral casing to the outlet of draft tube. In the following sections the pressure fluctuation prediction has been made at several positions of the turbine.

Table 1 Model Francis turbine parameters (n_s=252(m·Kw))

Specific speed	n_S=252 (m Kw)	Specific speed coefficient	K=1942
Runner diameter	D_1=350mm	Runner outlet diameter	D_2=364.4mm
Runner blade number	Z_B=13	Angle of spiral case	Φ =345°
Guide vane number	Z_0=24	Height of stray vane	B_0=0.315D_1
Guide vane diameter	D_0=1.1875D_1	Height of draft tube	H_0=2.6D_1
Length of draft tube	L=4.625D_1	Type of draft tube	4H Elbow

3.1 Stator-Rotor Interaction Simulation in Turbine

Fig. 3-1 shows the position of pressure recording at the inlet of spiral casing (S.C.), stay vanes (S.V.), guide and runner (G.V.). The pressure fluctuation at the position in front of runner will reflect the Stator-Rotor Interaction beween the guide vanes and runner of the turbine.

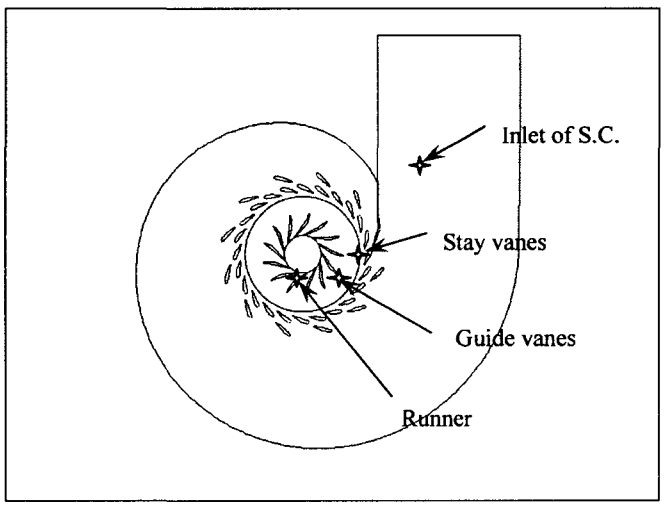

Fig. 3-1 Recording positions of pressure

Table 2 shows the unsteady computation results of the pressure fluctuation in front of runner at the small flow discharge condition (n_{11}=100r/min, a_0=16mm). Both amplitude (percentage of the water head of the turbine) and frequency (Hz) of pressure fluctuation are indicated at four points. The amplitude of pressure fluctuation at the four points has not much difference. The absolute values of the fluctuation is not high. And more higher the amplitude, more close to the runner the position. The frequency of fluctuation is a half of the rotating frequency of the runner.

Table 2 The pressure fluctuation in front of runner

	Inlet of S.C.		Stay vanes		Guide vanes		Runner	
condition	Amp.	Fre.	Amp.	Fre.	Amp.	Fre.	Amp.	Fre.
a_0=16mm	1.3%	13.0Hz	2.2%	13.0Hz	2.4%	13.0Hz	4.8%	13Hz

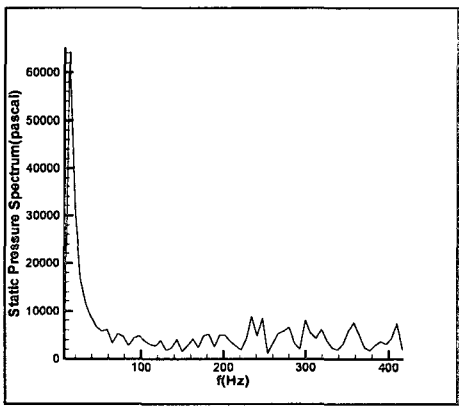

Fig. 3-2 Pressure spectrum at inlet of S.C. (n_{11}=100 r/min, a_0=16mm)

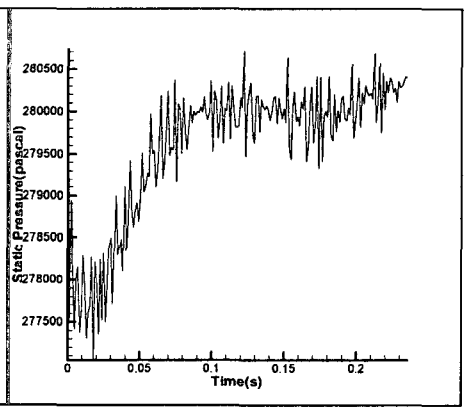

Fig. 3-3 Pressure versus time at inlet of S.C. (n_{11}=100 r/min, a_0=16mm)

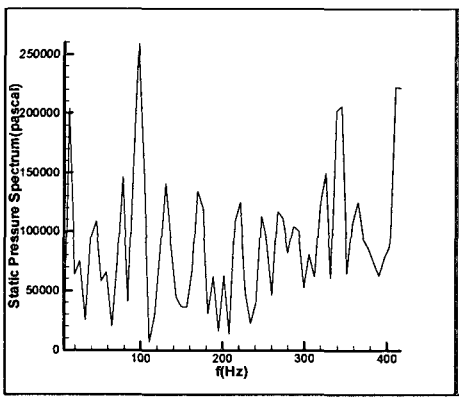

Fig. 3-4 Pressure spectrum at front of S.V. (n_{11}=100 r/min, a_0=16mm)

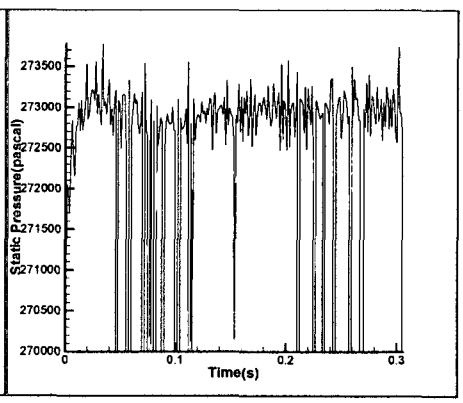

Fig. 3-5 Pressure versus time at front of S.V. (n_{11}=100 r/min, a_0=16mm)

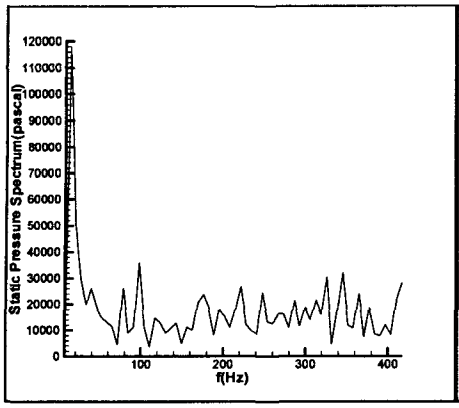

Fig. 3-6 Pressure spectrum at at front of G.V. (n_{11}=100 r/min, a_0=16mm)

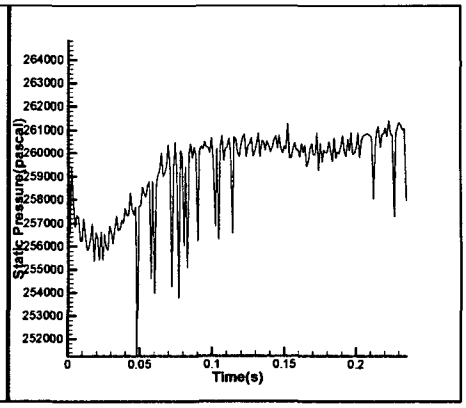

Fig. 3.-7 Pressure versus time at front of G.V. (n_{11}=100 r/min, a_0=16mm)

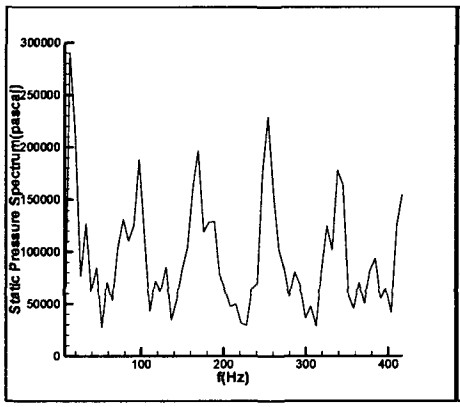

Fig. 3-8 Pressure spectrum at front of runner (n_{11}=100 r/min, a_0=16mm)

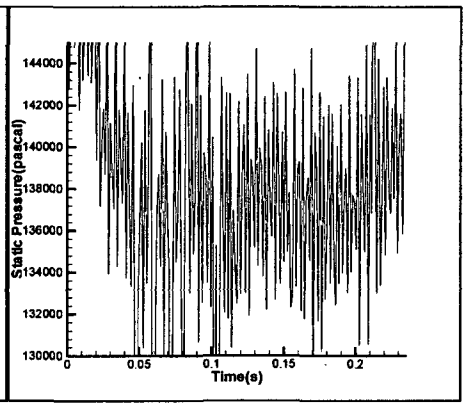

Fig. 3-9 Pressure versus time at front of runner (n_{11}=100 r/min, a_0=16mm)

3.2 Vortex Screw Rope Simulation in draft tube

Table 3 shows the pressure fluctuation at X-direction point (at upstream side) and Y-direction point (downstream side) at the inlet of the draft tube of the Francis turbine under the operation conditions of n_{11}=100r/min , a_0=16mm(Small flow discharge)and n_{11}=67r/min , a_0=24mm(large flow discharge).

Table 3 Pressure fluctuation at draft tube

Condition	Amp. at X	Amp. at Y	Fri. at X	Fri. at Y
n_{11}=100r/min a_0=16mm	6.4%	5.5%	13.0	13.0
n_{11}=67r/min a_0=24mm	4.0%	4.3%	9.0	8.8

Fig. 3-10 to 3-13 show the spectrum and amplitude versus time of pressure fluctuation at X-point and Y-point in the draft tube at small discharge condition (n_{11} = 100r/min, a_0=16mm), and Fig. 3-14 to 3-17 the results at large flow condition (n_{11} = 67r/min, a_0=24mm). The frequency of the pressure

fluctuation is a half of the rotating frequency of the runner. At the small flow condition the amplitude of pressure fluctuation is higher than that at large flow condition, which agrees with test data.

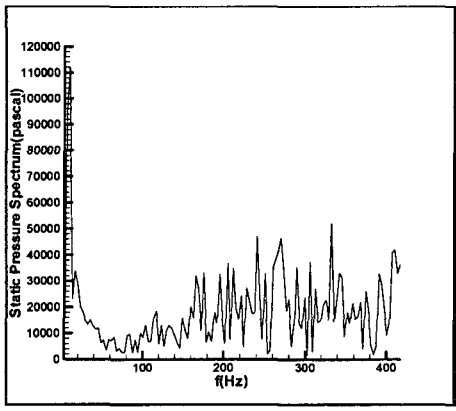

Fig. 3-10 Pressure spectrum at X point (n_{11}=67 r/min, a_0=24mm)

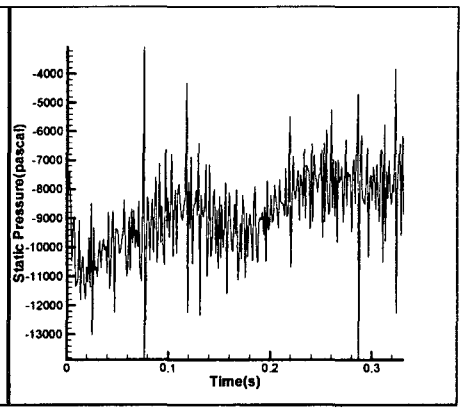

Fig. 3-11 Pressure versus time at X point (n_{11}=67 r/min, a_0=24mm)

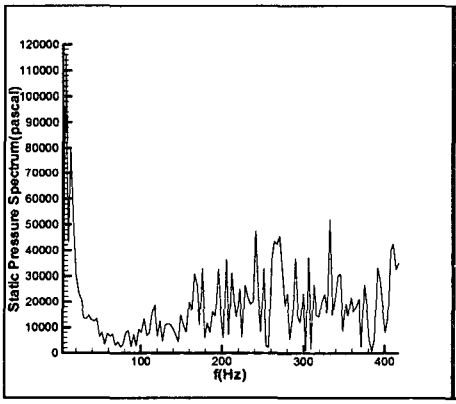

Fig. 3-12 Pressure spectrum at Y point (n_{11}=67 r/min, a_0=24mm)

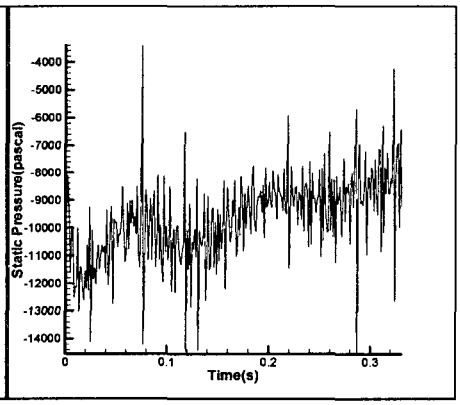

Fig. 3-13 Pressure versus time at Y point (n_{11}=67 r/min, a_0=24mm)

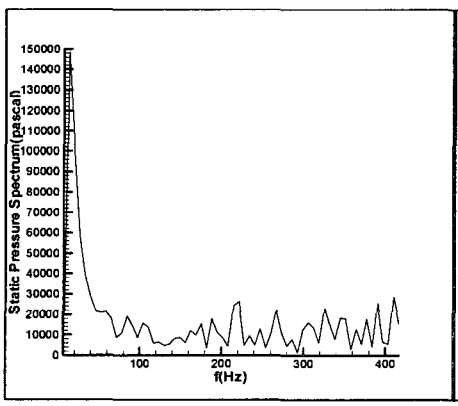

Fig. 3-14 Pressure spectrum at X point (n_{11}=67 r/min, a_0=24mm)

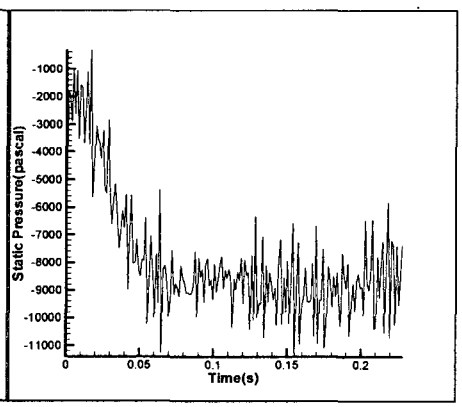

Fig. 3-15 Pressure versus time at X point (n_{11}=67 r/min, a_0=24mm)

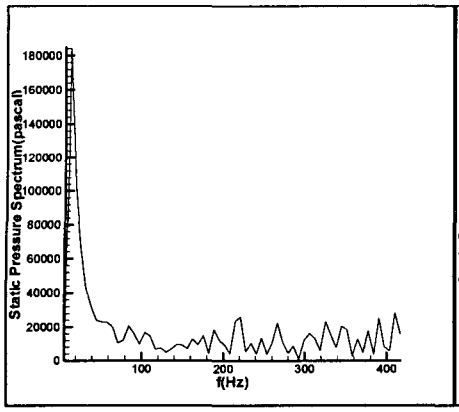

Fig. 3-16 Pressure spectrum at Y point (n_{11}=67 r/min, a_0=24mm)

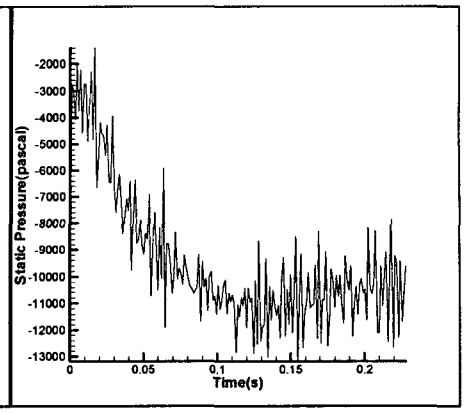

Fig. 3-17 Pressure versus time at Y point (n_{11}=67 r/min, a_0=24mm)

Fig. 3-18 indicates the pressure contour at inlet of draft tube at different time step at small flow condition (n_{11}=100 r/min, a_0=16mm), while Fig. 3-19 and Fig. 3-20 indicate the pressure contour at transverse sections and vertical sections respectively of draft tube at a time at small flow condition (n_{11}=100 r/min, a_0=16mm). The rotating direction of the vortex rope at small flow condition is the same as the rotation direction of runner of the turbine.

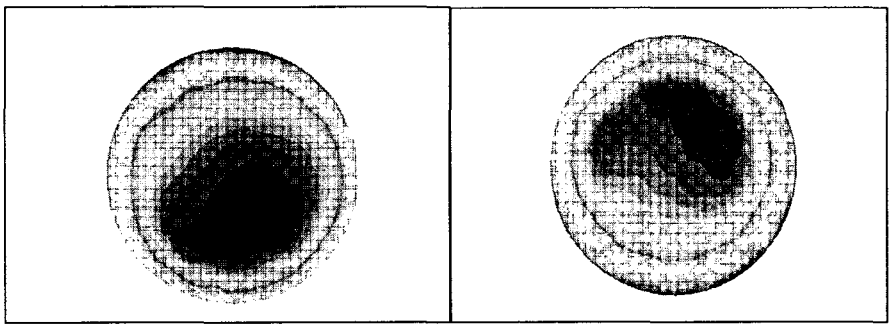

t=0s t=0.06s

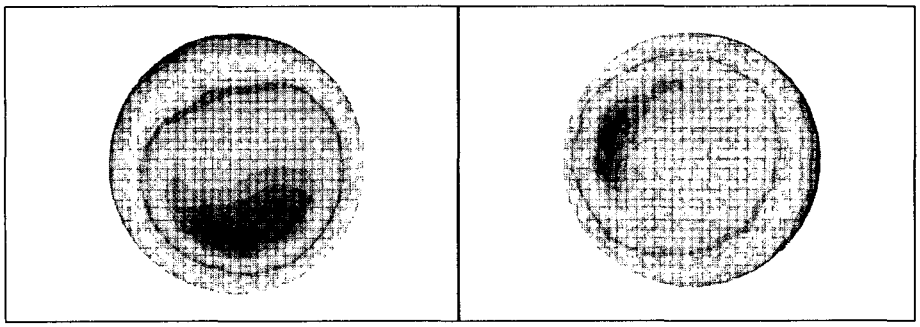

t=0.12s t=0.18s

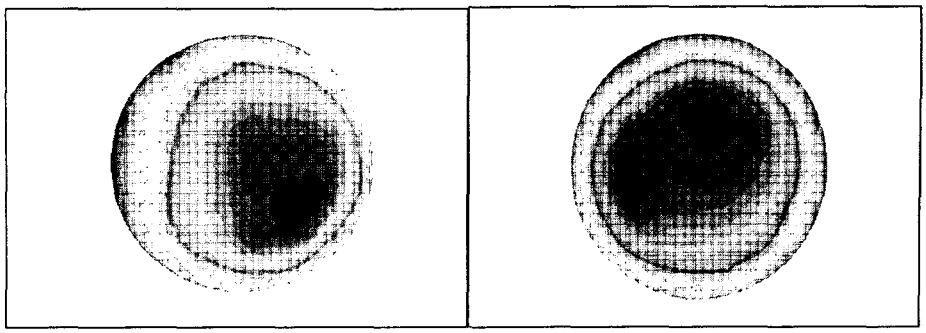

t=0.24s t=0.30s

Fig. 3-18 Pressure contour at draft tube inlet at different time step at condition (n_{11}=100 r/min, a_0=16mm)

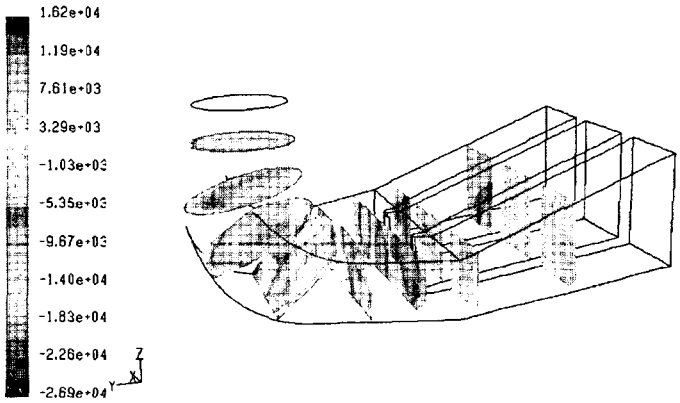

Fig. 3-19 Pressure contour at transverse sections of draft tube at a time at small flow condition (n_{11}=100 r/min, a_0=16mm)

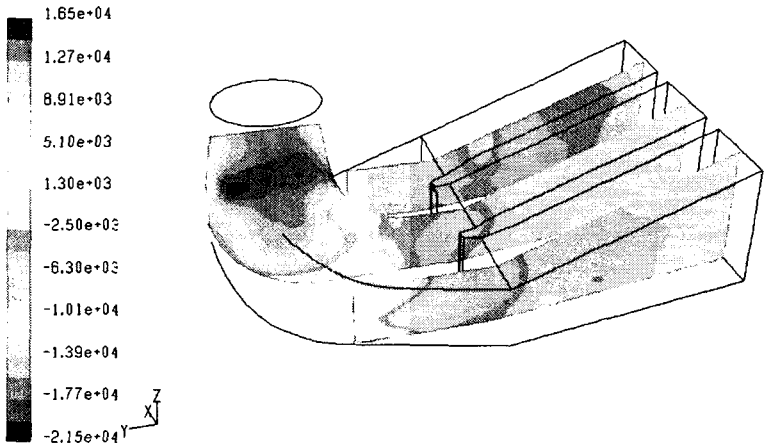

Fig. 3-20 Pressure contour at vertical sections of draft tube at a time at small flow condition (n_{11}=100 r/min, a_0=16mm)

Fig. 3-21 indicates the pressure contour at inlet of draft tube at different time step at large flow condition (n_{11}=67 r/min, a_0=24mm), while Fig. 3-22 and Fig. 3-23 indicate the pressure contour at transverse sections and vertical sections respectively of draft tube at a time at this flow condition. The rotating direction of the vortex rope at large flow condition is reverse to the rotation direction of runner.

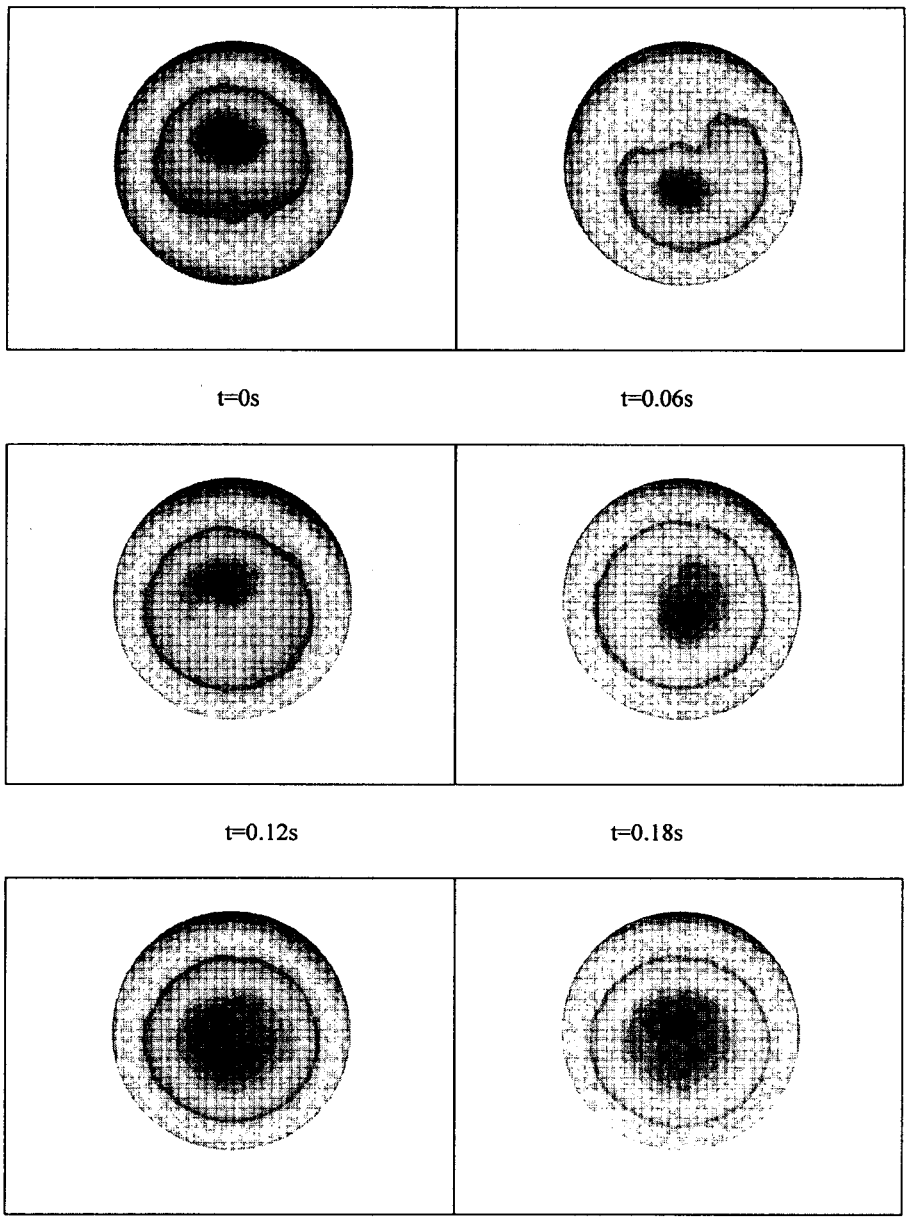

Fig. 3-21 Pressure contour at inlet of draft tube at different time step at large flow condition (n_{11}=67 r/min, a_0=24mm)

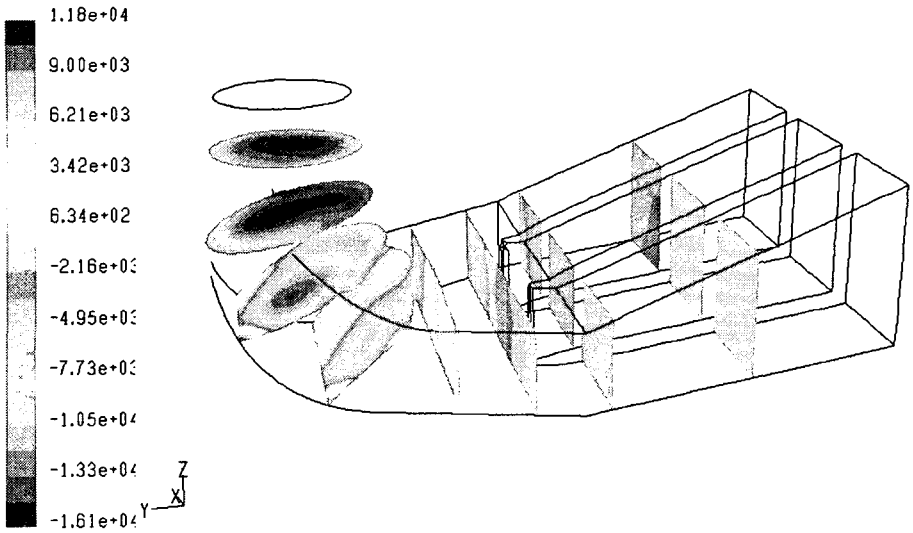

Fig. 3-22 Pressure contour at transverse sections of draft tube at a time at large flow condition (n_{11}=67 r/min, a_0=24mm)

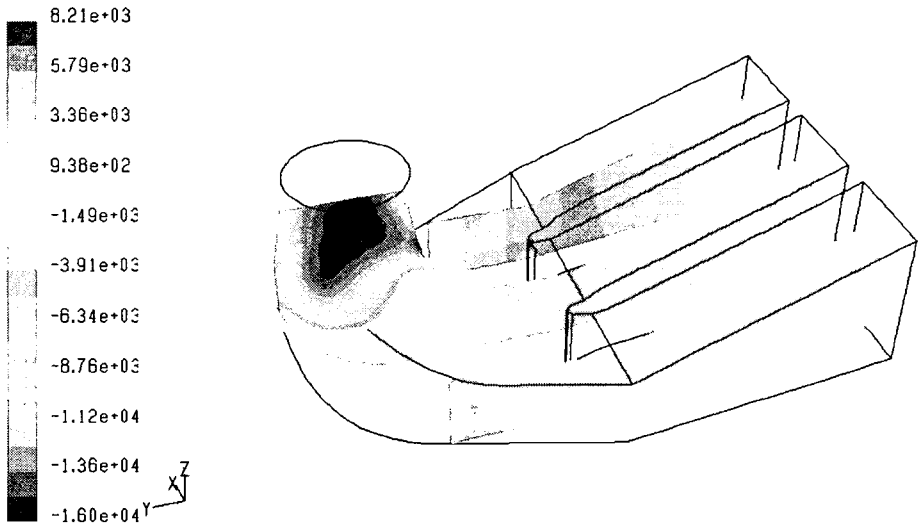

Fig. 3-23 Pressure contour at vertical sections of draft tube at a time at large flow condition (n_{11}=67 r/min, a_0=24mm)

3.3 Vortex Simulation through Runner

3.3.1 Passage vortex through the channel of runner

In Francis turbine, at off-design operation conditions the flow separation will occur near leading edges of runner blades, which induces the vortex through the channel of runner. For example, at low

water head condition there is a negative attack angle of flow at the leading edge of runner blade. Then the flow separation will exist near pressure surface of the blade. As the separation develops in the channel of the runner, the passage (channel) vortex will continue to exist till exit of the runner. In contrast, at high water head condition there is a negative attack angle of flow and the flow separation exists near suction surface of blade. The passage vortex is not stable, and induces the pressure fluctuation in the runner and also produces the vortex rope at the inlet of draft tube.

The unsteady calculation of the entire flow passage of a prototype hydraulic turbine has been carried out in the same way as the foregoing. The design water head is 140 m and the rated output is 700MW.

Fig.3-24 to Fig.3-26 show the flow trajectory through runner channel at condition of a low water head H=107m, and at the opening of guide vane (model test sizes), a_0=16mm, 18mm and 22mm. From those figures, there are channel vortex from the inlet to the outlet of the passage of runner. Because those results are at low head condition, the separation starts from the leading edge of pressure surface of runner blade. Because the blade of the Francis runner is X-type, the separation near the suction blade surface is limited. So that only at low head condition there is the channel vortex in the runner.

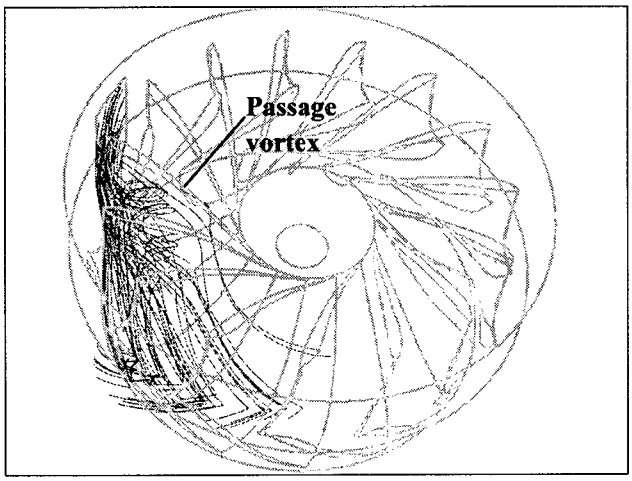

Fig.3-24a Flow trajectory through runner channel at condition of H=107m, a_0=16mm

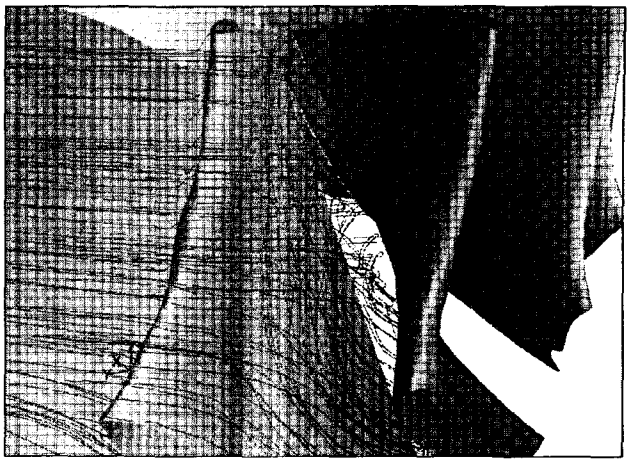

Fig.3-24b Detail trajectory through runner channel at condition of H=107m, a_0=16mm

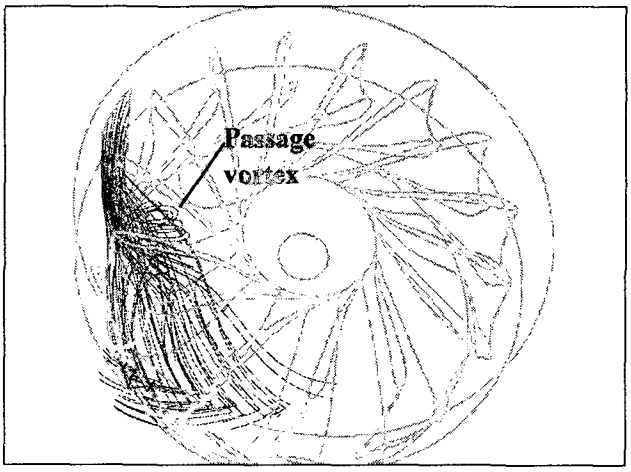

Fig. 3-25a Flow trajectory through runner channel at condition of H=107m, a_0=18mm

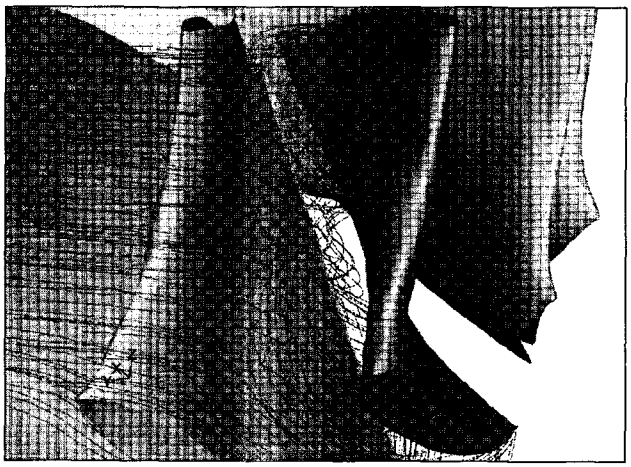

Fig. 3-25b Detail trajectory through runner channel at condition of H=107m, a_0=18mm

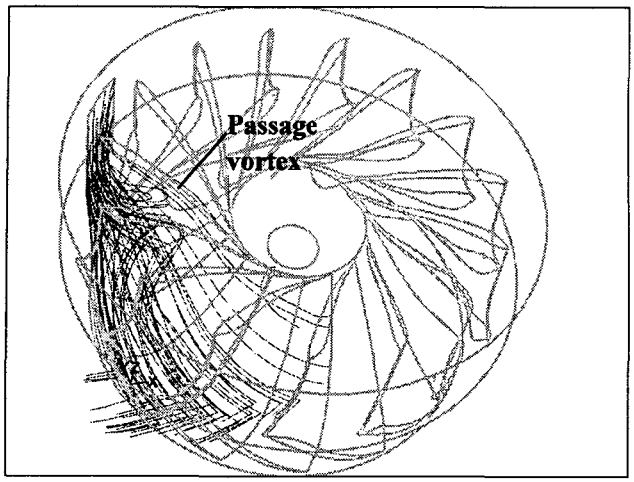

Fig. 3-26a Flow trajectory through runner channel at condition of H=107m, a_0=22mm

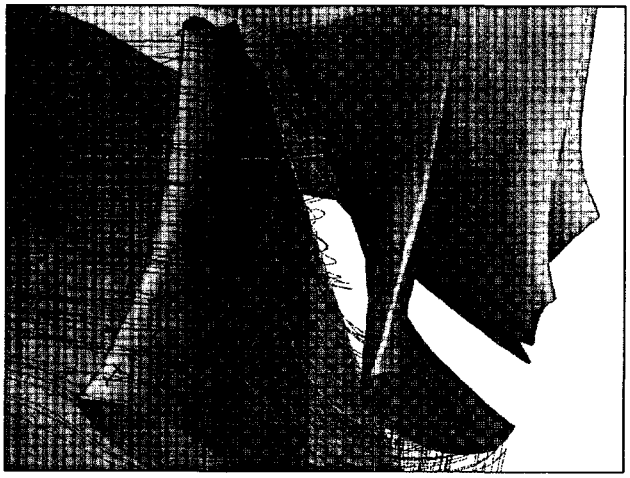

Fig. 3-26b Detail trajectory through runner channel at condition of H=107m, a_0=22mm

3.3.2 Eddy distribution of passage vortex through the channel of runner

The eddy components Ω_x, Ω_y and Ω_z of passage vortex through the channel of runner can be calculated as follows

$$\Omega_x = \frac{\partial w}{\partial y} - \frac{\partial v}{\partial z} \qquad \Omega_y = \frac{\partial u}{\partial z} - \frac{\partial w}{\partial x} \qquad \Omega_z = \frac{\partial v}{\partial x} - \frac{\partial u}{\partial y}$$

$$\Omega = \sqrt{\Omega_x^2 + \Omega_y^2 + \Omega_z^2}$$

where u, v and w are the components of velocity along x, y and z ordinate.

Fig. 3-27 to Fig. 3-29 show the eddy distribution at vertical section of radius R=3.0m in the runner channel at condition of H=107m and a_0=16mm, 18mm and 22mm respectively. Of course the

absolute values of eddy will increase with the increase of the flow rate. The relative values of eddy divided by the flow discharge are also calculated and listed in table 4. Table 4 shows the averaged eddy in runner channel at H=107m condition, but different guide vane openings from a_0=16mm to a_0=28mm. The value of Ω/Q is largest at small flow condition, that is, at a_0=16mm condition. At that condition the separation is strong and so is the relative eddy and the fluctuation of pressure in draft tube.

At the same time, the radius of the strongest eddy to the axis is larger at the condition of a_0=16mm, that means the channel vortex is largest at this condition. At other large opening conditions the size of the channel vortex will be smaller than that at smallest opening condition.

Table 4 Averaged eddy in runner channel at H=107m

Condition (guide vane opening)	Strong vortex dia. R (m)	Av.eddy $\Omega(s^{-1})$	Discharge Q(m^3/s)	Relative eddy Ω/Q	Pressure fluctuation in draft tube
a_0=16mm	3.0	60.9	260.446	0.2338	5.7%
a_0=18mm	3.0	66.1	289.175	0.2286	6.3%
a_0=22mm	2.8	74.2	351.054	0.2114	3.6%
a_0=26mm	2.6	85.5	414.317	0.2064	4.0%
a_0=28mm	2.6	95.6	461.613	0.2071	3.1%

Fig. 3-27 Eddy distribution at vertical section of radius R=3.0m in the runner channel at condition of H=107m , a_0=16mm

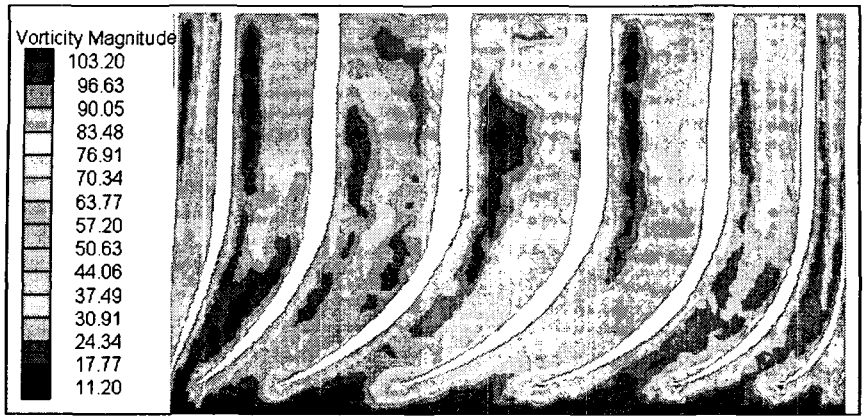

Fig. 3-28 Eddy distribution at vertical section of radius R=3.0m in the runner channel at condition of

H=107m , a_0=18mm

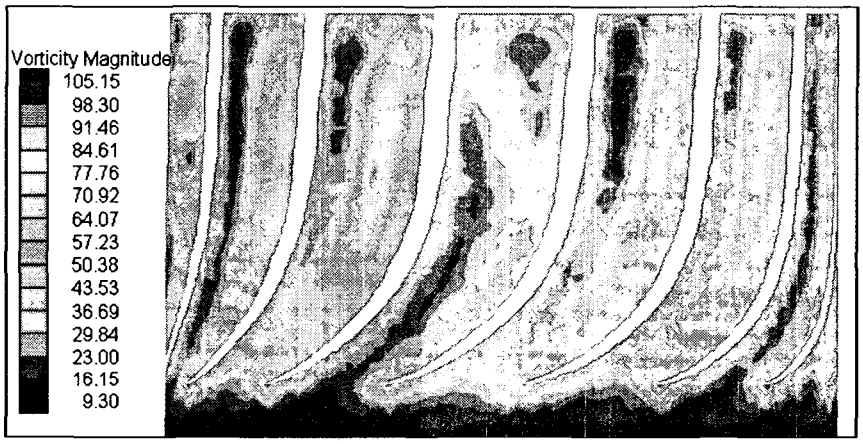

Fig. 3-29 Eddy distribution at vertical section of radius R=3.0m in the runner channel at condition of

H=107m , a_0=22mm

3.4 Comparison between Predicting Results and Test Data

3.4.1 Pressure fluctuation at front of runner of the model Francis turbine

From the results of pressure fluctuation at front of runner of the model Francis turbine at last sections, the closer the position is to the runner, the higher the amplitude of pressure fluctuation. The main frequency is the same as that in draft tube, that means the fluctuation is produced by transmitting of prossure fluctuation at the draft tube.

There are other character frequencies at the flow passage in front of runner. For example, at the small flow condition of n_{11}=100r/min and a_0=16mm, the frequencies 313 Hz, 234 Hz and157 Hz are one, 2/4 and 1/4 time of the product of multiplying the blade number of stay vanes with rotating frequency in front of stay vanes. At the same small flow condition, the frequencies 339 Hz, 254 Hz

and150 Hz are one, 3/4 and 1/2 time of the product of multiplying the blade number of runner with rotating frequency in front of turbine runner

3.4.2 Pressure fluctuation at draft tube of the model Francis turbine

Table 5 is the comparison of test data and calculated results of unsteady simulation by using different turbulence models, the RNG $k-\varepsilon$ and the standard $k-\varepsilon$ model at three operation conditions.

Table 5 Comparison of test data and calculated results

Condition			At inlet of spiral casing			At downstream side of inlet of draft tube		
			$\overline{A}_1$ (%)	f_1 (Hz)	f_1/f_n	$\overline{A}_2$ (%)	f_2 (Hz)	f_2/f_n
n11=100r/min, a0=16mm	Cal. results	$k-\varepsilon$	1.2	6.5	0.25	2.0	6.5	0.25
		RNG	1.3	13.0	0.50	5.5	13.0	0.50
	Test data		2.4	4.6	0.22	6.9	4.6	0.22
n11=78r/min, a0=18mm	Cal. results	$k-\varepsilon$	0.9			1.4		
		RNG	1.1			1.7		
	Test data		1.0			1.2		
n11=72r/min, a0=24mm	Cal. results	$k-\varepsilon$	1.0	4.7	0.25	3.9	4.7	0.25
		RNG	1.2	9.4	0.50	4.1	9.4	0.50
	Test data		1.8	3.5	0.23	4.5	3.7	0.24

CONCLUSIONS

The pressure fluctuation can be predicted by the present unsteady turbulent flow simulation through the entire flow passage, the whole flow passage from inlet of spiral casing to outlet of draft tube, of Francis turbine. The predicted results by using the standard $k-\varepsilon$ turbulence model seem to agree well with the test data both at the draft tube and at the front of spiral casing of the model turbine.

ACKNOWLEDGMENT

This paper was supported by the Key Project of National Foundation of Natural Sciences in China (Project No. 90410019).

REFERENCES

[1] GAMM-Workshop on 3D Computation of incompressible internal flows, Lausanne, 1989, NNFM, Vieweg, 1993.

[2] Ruprecht, A., et al., Numerical Simulation of a Complete Francis Turbine Including Unsteady Rotor/stator Interactions, 20th IAHR Symposium on Hydraulic Machinery and Cavitation, Charlotte,

2000.
[3] Ruprecht, A., et al., Parallel Computation of Stator-Rotor Interaction in an Axial Turbine, ASME PVP Conference, CFD Symposium, Boston, 1999.
[4] Skotak, A., Draft Tube Swirl Flow Modeling, IAHR WG "The Behavior of Hydraulic Machinery under Steady Oscillatory Conditions", Brno, 1999
[5] Kim S.-W., Chen, C.-P., A Multiple-time-scale Turbulence Model Based on Variable Partitioning of the Turbulent Kinetic Energy Spectrum, Numerical Heat Transfer 16(B), 1989.
[6] Ruprecht, A., "Unsteady Flow Analysis in Hydraulic Turbomachinery" 2002 IAHR I4.
[7] Kaechele T., Hauff C., Aschenbrenner T., Discussion of Several Numerical Approaches for the Stator-Rotor Interaction, Proceedings of the Hydraulic Machinery and Systems 21st IAHR

Symposium , September 9-12, 2002, Lausanne

[8] Song C.C.S., Compressibility Boundary Layer Theory and Its Significance in Computational Hydrodynamics, *Journal of Hydrodynamics*, Series B, Vol. 8, No. 2, 1996, pp. 92-101.
[9] Song, C.C.S., He, J. and Chen, X., Recent advancement in Computational Hydrodynamics Through Better Theoretical Bases, *XIX IAHR Symposium on Hydraulic Machinery and Cavitation*, Singapore, 1998.
[10] Chen X., Song C.C.S., Tani K., Shinmei, Niikura K. & Sato J., Simulation of Pressure Fluctuations in Pump-Turbines Induced by Runner-Guide Vane Interactions, Proceedings of the

Hydraulic Machinery and Systems 21st IAHR Symposium , September 9-12, 2002, Lausanne.